Quantifying Argon Concentration within Insulating Glass Units using Low Frequency Ultrasonic Technique

Hamed Khaleghi*, Parisa Salehi, Chenxi Xu, Didem Ozevin, Aslihan Karatas

Department of Civil, Materials and Environmental Engineering, University of Illinois Chicago, 842 W Taylor St., Chicago, IL, 60607, United States

Abstract

Insulating glass units (IGUs) account for over 30% of thermal transmission losses in building envelopes. To mitigate this, IGUs are often filled with low-conductivity gases like Argon. However, Argon concentration decreases over time due to IGU aging and manufacturing processes, which lessens their insulating effectiveness. This study presents a novel nondestructive methodology to quantify Argon concentration in IGUs using ultrasonic technique. The ultrasonic energy transmitted through the IGU is correlated with Argon concentration, validated through both experimental measurements and numerical models using COMSOL Multiphysics®. The models simulate acoustic-structure interaction by adjusting gas density to reflect Argon presence, showing increased ultrasonic energy with higher Argon concentrations. Experimental measurements on two IGU samples with twenty Argon-air mixtures (ranging from 100% to 25% Argon) show that the proposed ultrasonic technique achieves a mean absolute error of 0.13, outperforming Spark Emission Spectroscopy and Helantec ISO-GAS-Control, which have errors of 2.31 and 0.33, respectively.

Keywords: Argon-air gas mixtures; Gas analyzer; Ultrasonic energy; Non-destructive evaluation; Double-pane windows

Introduction

In the United States, residential and commercial buildings account for over 40% of primary energy consumption and 70% of electricity use, leading to annual energy costs exceeding $430 billion, with approximately 35% of this consumption attributed to losses through the building envelope (Watts et al. 2022). Within building envelopes (e.g., walls, windows, foundation, and roofs), windows account for up to 60% of a building's total energy loss, due to: (1) high U-values compared to opaque envelope components such as walls and (2) solar heat gain that contributes to overall heat transfer into indoor spaces (Cuce and Riffat 2015; Gustavsen et al. 2007; Jelle et al. 2012; Lee et al. 2021; Likins-White et al. 2023). Therefore, even minimal improvements in window performance can significantly enhance buildings' energy efficiency.

In the past few decades, double-pane windows, also known as insulating glass units (IGUs), have been installed to replace single-pane windows to improve windows' overall performance (i.e., reduce energy consumption for heating and cooling and provide a comfortable indoor environment for occupants) (Samaitis et al. 2022; Selkowitz et al. 2018). This improvement results from two major modifications: (1) applying low-e coatings on the surface of glass panes (i.e., lites) to reduce solar heat gains and infrared heat transfer (Lolli and Andresen 2016; Papaefthimiou et al. 2006; Peng et al. 2021); and (2) utilizing heavy inert gases (i.e., Argon, Krypton, Xenon) to fill the cavity

between the lites of IGUs to reduce convective heat transfer due to heavy inert gases' lower thermal conductivity (Ghazi Wakili et al. 2021; Respondek 2020; Savić et al. 2013; Van Den Bergh et al. 2013). It should be noted that although low-e coatings can solely reduce the U-value of IGUs (Bizoňová and Bagoňa 2019), achieving the low U-values required by the NPR-CEN ISO 2017 standard is not feasible without utilizing Argon within the IGU spacers (van Nieuwenhuijzen et al. 2023).

Among the heavy inert gases for windows, Argon is the most commonly used for IGUs due to its optimal balance of cost-effectiveness and thermal performance. It is considerably less expensive than Krypton and Xenon, yet it offers effective insulation by reducing convective heat transfer between lites. Moreover, Argon is non-toxic and widely available, making it a practical choice for improving the overall performance of IGUs and it is non-toxic and readily available making it a practical choice for enhancing the overall performance of IGUs (Cuce and Riffat 2015; Miskinis et al. 2015; Respondek 2020; Summ et al. 2023). Despite the benefits of Argon-filled IGUs, a critical issue emerges over time - the leakage of Argon from IGUs, leading to a degradation of their insulating capabilities and, consequently, a compromise on their performance and energy efficiency potential (Knorr et al. 2016).

EN 1279-3 (2018) mandates that IGUs must maintain a gas loss rate of no more than 5% over 25 years. This requirement is essential because an Argon gas filling below 80% can significantly degrade the thermal performance of the IGU (i.e., worse U-value) and compromise its anticipated 25-year lifespan (van Nieuwenhuijzen et al. 2023; Wolf 2002). However, Argon loss within IGUs is unavoidable for two primary reasons: (1) Argon gas concentration naturally diminishes over time due to the gradual degradation of primary and secondary sealing materials, driven by environmental factors such as atmospheric pressure fluctuations, temperature variations, and solar radiation; and (2) potential operational errors during the manufacturing, handling, or transportation of IGUs (Knorr et al. 2016; Likins-White et al. 2023; Respondek 2020; Samaitis et al. 2022; Summ et al. 2023). Therefore, Argon gas leakage within IGUs could be a serious problem due to: (1) leading to thermal performance loss (resulting in higher U-values); (2) compromising moisture resistance (leading to condensation and mold growth issues); and (3) diminishing sound-blocking performance (resulting in a noisier indoor environment).

A reduction in Argon concentration within IGUs directly results in diminished thermal performance, as indicated by increased U-values. Asphaug et al. (2016) examined the influence of the aging of IGUs on the reduction in Argon concentration within the IGU's spacer. They discovered that as IGUs age, the Argon concentration decreases from 92.7% to 46.3%, leading to a 12% decrease in thermal performance, as evidenced by a change in U-value from 1.18 W/m²K to 1.32 W/m²K. Cho et al. (2023) demonstrated a 10.9% reduction in the thermal performance of IGUs when the Argon gas filling rate dropped from 95% to 0%. Furthermore, they found a 92% probability that the Argon gas filling rate in double-glazed IGUs would decrease below 65% within two years, leading to a 4.3% loss of insulation.

Argon loss also affects the acoustic performance of IGUs. Sound energy transmission in a material occurs through the vibration of the material, and this process is influenced by the material's mass and the sound frequency. An increase in mass enhances sound insulation due to greater inertia

forces, resulting in improved acoustic insulation properties (Bliūdžius et al. 2022). The sound transmission loss (TL), which is the main indicator of the acoustic performance of IGUs, depends on various factors, including the number and thickness of lites, glass and coating type, sealing type, and filling gas (Rasmussen and Gerretsen 2014; Tadeu and Mateus 2001). Findings by Zhu et al. (2024) and Miskinis et al. (2015) have shown that Argon-filled IGUs exhibit twice the TL at a similar frequency range compared to air-filled IGUs.

Another frequent challenge associated with Argon loss in IGUs is the increased relative humidity resulting from the replacement of Argon with air, especially in tropical or subtropical climates. The excessive moisture and oxygen within the air in the IGU's spacer can initiate reactions with other parts of IGU, such as with the secondary silicone sealant, accelerating its deterioration and consequently compromising the IGU's performance (Abraham et al. 2023). Additionally, the moisture increases the possibility of mold growth, resulting in damage to window frames and surrounding walls. This process accelerates the degradation of the building envelope and diminishes indoor air quality, which leads to allergic reactions in occupants (Rogers 2010).

These factors collectively result in higher replacement costs, occupant discomfort, and elevated CO_2 emissions associated with the overall energy consumption of buildings (Kim and Kim 2019; Souviron et al. 2019; Zier et al. 2021). Therefore, measuring the Argon concentration within IGUs becomes essential for the building sector to optimize the long-term efficiency of IGUs and identify the most effective retrofit strategies, considering that the lifespan of buildings significantly exceeds that of IGUs (El-Darwish and Gomaa 2017; Likins-White et al. 2023; Rodrigues and Freire 2017).

Available Methodologies for Argon Quantification in IGUs

Quantifying the Argon concentration within IGU spacers can be achieved through several methodologies, including destructive and non-destructive approaches. Destructive approaches to measure Argon concentration within IGUs include Gas chromatography (GC) and gas analyzers, which typically utilize thermal conductivity detectors (Haglin 2021). Gas chromatography operates based on separating and detecting different gas components within the sample mixture (Cramers et al. 1999; Lasa et al. 2002), while gas analyzers operate based on the difference in thermal conductivity of gas mixtures (Helantec ISO-GAS-Control). These destructive approaches involve breaching the seal to extract a gas sample, which is then injected into a GC or gas analyzer. Although these methods exhibit high accuracy, making them suitable for laboratory settings and quality control during manufacturing, their dependence on breaching the seal to extract a gas sample makes them inherently destructive, limiting their applicability to IGUs installed on-site due to the inaccessibility of the sides of installed units (van Nieuwenhuijzen et al. 2023).

Non-destructive approaches include three different methodologies to measure Argon and/or Krypton concentrations within IGUs: (1) Spark Emission Spectroscopy (SES); (2) Tunable Diode Laser Absorption Spectroscopy (TDLAS); and (3) Ultrasonic Testing (UT). The first methodology (i.e., SES), a high voltage (approximately 50000V) at low current is applied to the glass surface, creating a spark that induces plasma from the gas molecules within the IGU. This process results in the emission of light photons at characteristic wavelengths. The device collects and analyzes these photons via spark emission spectroscopy, comparing the resulting spectrum to internal calibration data to determine the Argon concentration within the IGU (Sparklike Handheld™

2024). The SES methodology is limited to IGUs with glass lite thicknesses ranging from 2 to 6 mm and spacer thicknesses between 6 and 20 mm. The second methodology, TDLAS, determines the amount of oxygen present within the IGU spacer. Subsequently, it calculates the insulating Argon and/or Krypton concentration based on the known ratio of air gas components (Sparklike Laser Portable™ 2024; Ghazi Wakili et al. 2021). The spacer's width is factored into this calculation, along with the oxygen content (van Nieuwenhuijzen et al. 2023).

The third methodology, ultrasonic testing (UT), involves transmitting low to high-frequency elastic waves into the IGU spacer and analyzing the reflected waveforms (Zhang 2024). UT has been utilized to quantify the Argon concentration within IGU spacers (Butkus et al. 2004; Glora et al. 1999; Jedrusyna and Noga 2016; Samaitis et al. 2022). Existing studies have utilized UT to determine Time of Flight (ToF) values, which indicate the time taken by ultrasonic waves to travel a specific distance within a medium (Hoseini et al. 2012). This method is based upon the differences in ultrasound velocity between different gases, leveraging the inherent contrast in velocity between air and heavy inert gases (e.g., Argon, Krypton, or Xenon). Since ultrasound travels faster in the air, the presence of a heavy inert gas reduces the sound velocity within the IGU spacer (Taskin and Kato 2019). Therefore, to accurately measure ToF and determine the Argon concentration within the IGU spacer, two key variables must be precisely measured, the ultrasound velocity within the spacer and the thickness of the lites and spacers of the IGUs.

The ultrasound velocity depends on temperature and pressure variations, resulting in significant changes in measurements under different environmental conditions. For instance, within the temperature range of 15–25°C, a 1°C temperature change leads to a velocity shift of 0.6 m/s in air and 0.55 m/s in Argon (Butkus et al. 2004). Furthermore, the ultrasound velocity in Argon (319 m/s) is relatively close to that of air (343 m/s) when compared to Krypton (220 m/s) and Xenon (175 m/s) (Butkus et al. 2004; Glora et al. 1999). Glora et al. (1999) achieved a ±1% error in sound velocity measurement, resulting in an accuracy of ±20% for Argon-filled IGUs and ±5% for Krypton-filled IGUs in quantifying gas content. Therefore, it is challenging to differentiate between Argon and air even with precise estimation of ultrasound velocity for accurate determination of Argon concentration.

The aforementioned non-destructive methodologies enable Argon quantification without breaching the IGU seal, making them suitable for on-site measurements. These techniques provide rapid results and are valuable for monitoring gas retention in operational IGUs and performing quality control during manufacturing. However, they require expensive equipment that may not always be readily available due to limited manufacturing and accessibility. Additionally, their accuracy can be compromised by factors such as the thickness of IGU spacers and lites, the presence of low-e coatings, and Argon concentrations below 90%. Table 1 presents the available methodologies for measuring Argon concentration within IGUs, providing their accuracy and limitations.

Table 1. Available methodologies for measuring Argon concentration within IGUs

Methodology	Accuracy Range	Limitations

Helantec Gas Analyzer (Helantec ISO-GAS-Control 2024)	±0.6	Destructive, inaccurate below 30%
Gas Chromatography (Safavi et al. 2010)	N.A.*	Destructive, not accessible, requires skilled operators
Tunable Diode Laser Absorption Spectroscopy (Sparklike Laser Portable™ 2024)	±1.5	Expensive, limited availability, limited glass thickness, requires daily calibration
Spark Emission Spectroscopy (Sparklike Handheld™ 2024)	±1.5 (above 80% Argon) – ±3.5 (below 80% Argon)	Expensive, limited availability, less accurate below 80%, not applicable in presence of low-e
Hybrid Ultrasonic (Samaitis et al. 2022)	±3.5 (based on GC)	Requires high accurate sound velocity measurements

* The accuracy range of GC devices varies depending on the specific model and its intended application.

The aforementioned challenges highlight the ongoing need for inspection techniques that are rapid, non-intrusive, and low cost for quantifying Argon concentration within IGUs. Although UT demonstrates potential for meeting these requirements, existing methodologies rely on parameters such as IGU lite and spacer thickness, ultrasound velocity, and ToF, which are sensitive to environmental variations and measurement complexities. Moreover, accurate identification of ToF can be obscured by low signal-to-noise ratio of direct wave penetrating through solid-gas-solid interfaces and wave dispersion. In this study, a novel approach is presented that shifts the focus from these conventional parameters to UT waveform analysis, specifically the calculation of ultrasonic energy values, to quantify Argon concentration within the IGU spacer. This approach minimizes reliance on environmental factors and measurement complexities, instead focusing primarily on the internal Argon-air mixture composition of IGUs since the energy-based approach is less affected by these variables as it relies on the behavior of entire waveform through the direct path between the transmitter and the receiver transducers. Therefore, the proposed methodology addresses the limitations of current techniques outlined in Table 1, such as dependency on precise thickness and velocity measurements, while maintaining high accuracy and reducing measurement costs. By enabling non-invasive, rapid, and reliable Argon quantification, the proposed method significantly enhances the capability for in-use IGU performance assessment and supports improved quality control during manufacturing, maintenance, and operation. This study contributes a transformative tool to the on-site measurements, addressing critical gaps in existing research and advancing the practical applicability of non-destructive evaluation methods for IGUs.

Objective

This study aims to develop a non-destructive and accessible methodology to accurately measure Argon concentration within IGUs using the UT technique. To achieve this, the following steps are carried out: (1) utilizing an experimental setup that creates twenty different mixtures of Argon and air and transfers the mixtures to the spacers of two IGU samples; (2) performing UT measurements on the IGU samples with a 60kHz excitation frequency to generate UT waveforms; (3) analyzing ultrasonic waveforms to investigate the correlation between UT features and Argon concentration,

ultimately identifying ultrasonic energy as the primary indicator for measuring Argon concentration; (4) applying statistical methods to determine Argon concentration associated with the ultrasonic energy value of each Argon-air mixture; (5) implementing numerical model using COMSOL Multiphysics® (V6.0); (6) simulating IGU samples and UT waveforms in COMSOL Multiphysics® to validate the experimental results from the UT measurements; (7) measuring Argon concentration of IGU samples by other two methodologies including a commercial device Sparklike Handheld™ utilizing SES methodology (non-destructive approach) and a gas analyzer Helantec-ISO-Gas Control, HIGC (destructive approach); and (8) comparing the Argon concentration values derived from the three methodologies and assessing their performance by evaluating their error range.

Methodology

The proposed methodology in this study is divided into three main sections: (1) experimental analysis, (2) numerical analysis, and (3) comparison analysis across the three methodologies employed in this study to measure Argon concentration within IGU samples. These sections are separated into a total of eight steps (see Figure 1).

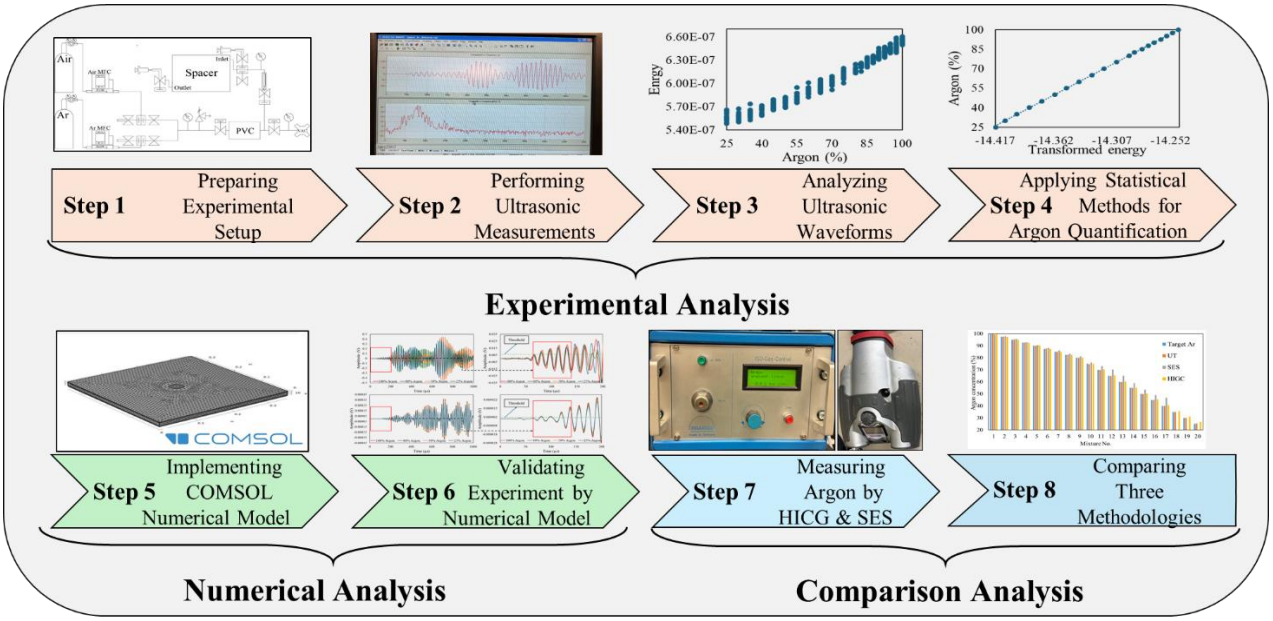

Figure 1. Stepwise procedure of quantifying Argon concentration within the IGU samples using the proposed UT methodology and comparing the results with the commercial device (SES) and gas analyzer (HIGC)

Section 1- Experimental Analysis

This section comprises four steps: (1) preparing experimental setup to create and transfer twenty Argon-air mixtures; (2) conducting UT measurements on each target Argon-air mixture; (3) analyzing UT waveforms to establish a correlation between UT features and Argon concentration; and (4) employing statistical methods to quantify Argon concentration within IGU samples based on the ultrasonic energy values. Each step for this section is detailed below:

Step 1: Preparing IGU Samples and Experimental Setup

In this study, two double-pane IGU samples were prepared for conducting UT measurements (see Figure 2). The first sample (referred to as IGU1) is a typical IGU with lateral dimensions of 420 mm by 470 mm and consists of two 2.4 mm lites with an 11.2 mm spacer. The second sample (referred to as IGU2) is manufactured with lateral dimensions of 350 mm by 350 mm and comprises two 4 mm lites with a 12 mm spacer. IGU2 is chosen for its similarity to the samples used in ASTM E2649-20 measurements, facilitating an accurate comparison between the proposed UT methodology and the SES methodology. Both IGU samples consist of one clear uncoated lite and one lite with a low-e coating (ASTM E2649-20).

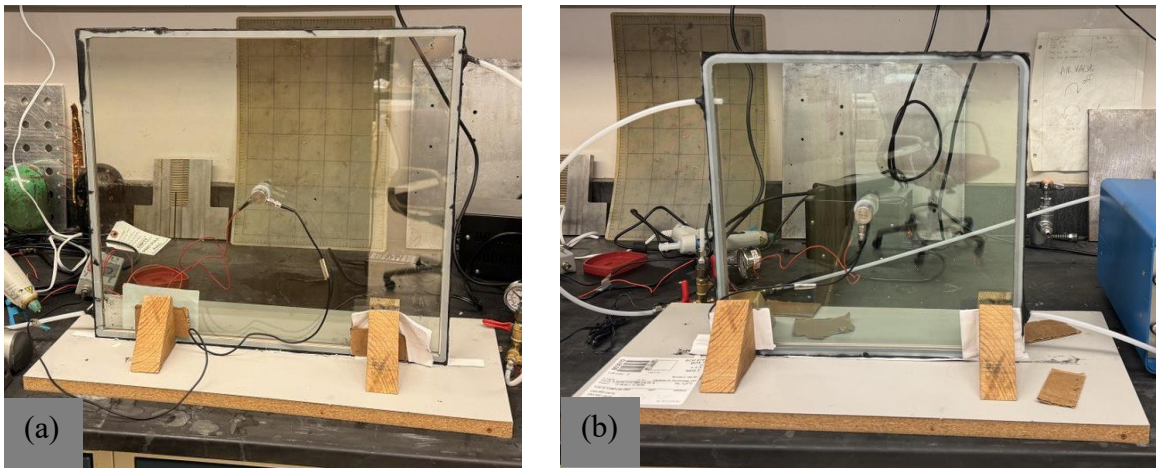

Figure 2. Tested IGU samples: (a) IGU1; (b) IGU2

To establish a methodology for measuring Argon concentration in IGU spacers, it is necessary to create various gas mixtures of Argon and air within the IGU spacer. Therefore, a total of twenty different Argon-air mixtures are created and injected into the IGU samples to evaluate the proposed UT methodology for measuring the Argon concentration. Connection tubes with an inner diameter of 4 mm and an outer diameter of 6 mm, are used for transferring the gas mixtures to the IGU samples. Butyl rubber strips are applied to seal the surrounding frame of the IGU samples, as well as the inlet and outlet, to prevent any air leakage during the experiment. Table 2 presents a list of targeted twenty Argon-air mixtures created for UT measurements in this study. The Helantec ISO-GAS-Control (HIGC) device with an accuracy of ±0.6% is employed for two purposes: (i) verifying the gas mixtures created by the Argon-air mixture experimental setup by extracting a gas sample before the inlet of the IGU samples and (ii) comparing the Argon concentration values obtained from UT measurements by extracting a gas sample after the outlet of the IGU samples.

Table 2. List of Argon-air target mixtures

Mixture No.	**1**	**2**	**3**	**4**	**5**	**6**	**7**	**8**	**9**	**10**	**11**	**12**	**13**	**14**	**15**	**16**	**17**	**18**	**19**	**20**
Argon (%)	100	97.5	95	92.5	90	87.5	85	82.5	80	75	70	65	60	55	50	45	40	35	30	25

As illustrated in Figure 3, the experimental setup for creating Argon-air mixtures involves four sequential stages: (1) calibration of the HIGC device using an Argon cylinder tank and an Argon

calibration bottle to verify the target gas mixtures of Argon and air (Figure 3a); (2) evacuation of the pressure/vacuum chamber (PVC) to establish a vacuumed environment for creating a precise Argon and air mixture (Figure 3b); (3) generation of the target Argon-air mixtures within the PVC using MC-Mass Flow Controllers[1] (MFCs) manufactured by Alicat Scientific, Inc. (Figure 3c); and (4) transfer of the target mixture from the PVC into the spacer of the IGU samples to perform the UT test. Two gas sampling spots are located before and after the IGU spacer to verify the Argon concentrations within the PVC and IGU spacer, respectively (Figure 3d). To maintain the stability of the Argon-air mixture during UT measurements, the inlet and outlet of the spacer are closed prior to the measurements, and a 30-second waiting period is provided to allow the gas mixture to settle. Moreover, to ensure the homogeneity of the mixture, the Argon-air mixture is prepared in PVC at 10 psi, ensuring uniform homogeneity within the IGU. Detailed information regarding the Argon-air mixture experimental setup and calibration process of HIGC device is explained in Khaleghi et al. 2025.

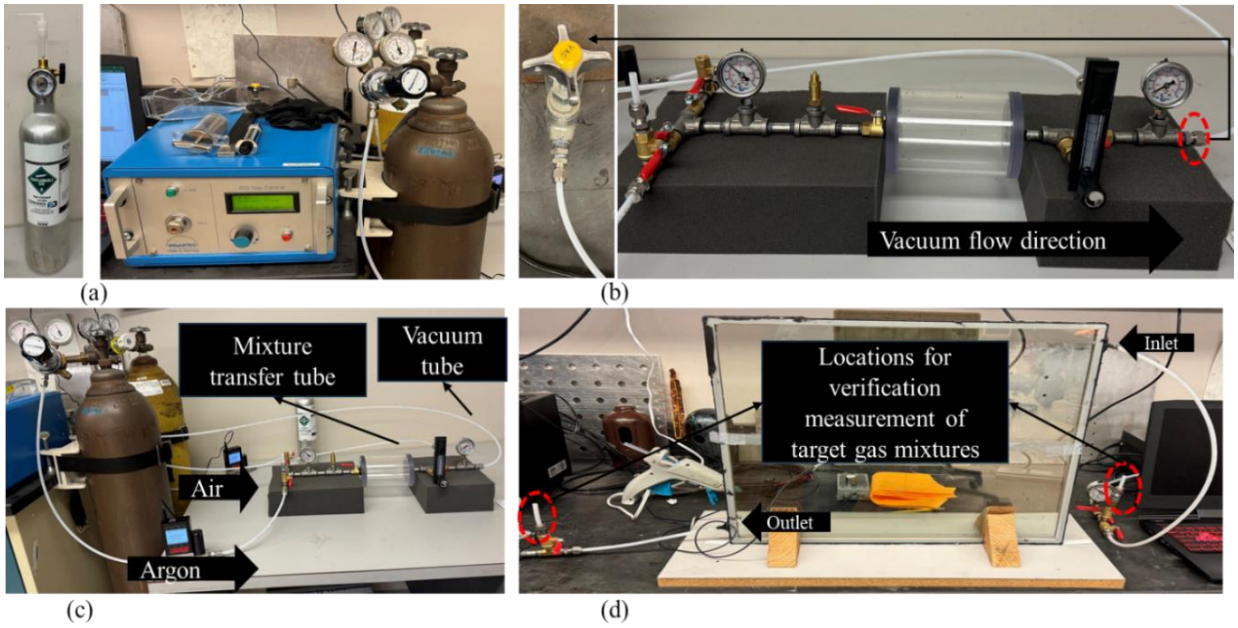

Figure 3. Overview of the Argon-air mixture experimental setup: (a) calibrating HIGC with Argon calibration gas bottle and Argon cylinder tank; (b) vacuuming PVC by vacuum valve; (c) generating Argon-air target mixtures within the PVC; (d) transferring the target mixture from the PVC to IGU spacer [Khaleghi et al. 2025]

Table 3 and Table 4 present the Argon concentration percentage values measured by HIGC device for the twenty Argon-air gas mixtures created by the experimental setup for injection into the IGU1 and IGU2, respectively. To ensure the accuracy of the Argon-air mixtures, the repeatability of the HIGC device, and the consistency of ultrasonic measurements (Step 3), the entire experiment is conducted in three replicates, and each Argon-air mixture is measured five times using the HIGC device.

[1] The MFC devices are identified by their respective serial numbers, MC-5SLPM-D MFC for Argon: 466868 and MC-1SLPM-D for air: 466864.

Table 3. Argon percentage values of the twenty Argon-air mixtures created for IGU1 (readings are obtained by HIGC)

Replicate 1 (IGU1)													
Argon target (%)	1	2	3	4	5	Avg	Argon target (%)	1	2	3	4	5	Avg
100.0	100.1	100.4	101.0	100.1	99.9	100.3	70.0	70.9	70.6	70.5	70.8	70.8	70.72
97.5	97.7	97.8	97.7	97.6	97.5	97.66	65.0	65.8	65.7	65.8	65.9	65.6	65.76
95.0	95.5	95.4	95.2	95.4	95.1	95.32	60.0	61.0	60.8	60.7	60.8	60.5	60.76
92.5	93.1	92.6	92.7	93.0	93.1	92.90	55.0	56.5	56.5	56.0	56.2	56.5	56.34
90.0	90.8	90.7	90.6	90.5	90.2	90.56	50.0	49.7	49.6	49.8	49.9	49.8	49.76
87.5	88.3	88.0	87.9	87.7	88	87.98	45.0	44.8	44.7	44.9	45.1	45.0	44.90
85.0	85.8	85.6	85.4	85.5	85.5	85.56	40.0	40.1	40.0	40.1	40.2	39.9	40.06
82.5	83.2	83.0	82.8	83.0	82.7	82.94	35.0	35.4	35.2	35.4	35.4	35.5	35.38
80.0	80.8	80.8	80.5	80.5	80.8	80.68	30.0	31.0	31.5	32.0	32.0	31.9	31.68
75.0	75.8	75.9	75.8	76.0	75.5	75.80	25.0	26.4	26.6	26.3	26.6	26.5	26.48
Replicate 2 (IGU1)													
Argon target (%)	1	2	3	4	5	Avg	Argon target (%)	1	2	3	4	5	Avg
100.0	100.3	100.4	100.1	100.0	100.0	100.1	70.0	68.9	69.8	69.8	68.8	70.0	69.46
97.5	97.8	97.5	97.5	97.8	97.6	97.64	65.0	63.5	65.2	64.8	64.7	64.9	64.62
95.0	95.2	95.0	95.2	95.0	95.0	95.08	60.0	60.0	59.6	59.8	59.6	60.0	59.80
92.5	92.4	92.3	92.5	92.6	92.5	92.46	55.0	54.8	54.7	54.8	54.8	54.8	54.78
90.0	89.8	89.9	90.0	89.9	89.8	89.88	50.0	50.0	49.8	50.0	50.0	49.9	49.94
87.5	87.3	87.0	87.2	87.3	87.1	87.18	45.0	45.0	44.9	44.8	45.0	45.9	45.12
85.0	84.4	84.3	84.3	84.5	84.3	84.36	40.0	39.9	40.0	39.9	39.8	40.0	39.92
82.5	82.3	82.6	82.4	82.7	82.5	82.50	35.0	35.0	34.9	35.2	35.0	34.7	34.96
80.0	79.3	80.0	79.2	79.6	79.8	79.58	30.0	31.7	31.5	31.6	31.6	31.7	31.62
75.0	74.1	74.8	74.9	75.0	75.2	74.80	25.0	26.3	26.5	26.0	25.9	25.7	26.08
Replicate 3 (IGU1)													
Argon target (%)	1	2	3	4	5	Avg	Argon target (%)	1	2	3	4	5	Avg
100.0	100.3	100.1	100	100.6	100.1	100.2	70.0	70.1	70.0	70.1	70.2	70.4	70.16
97.5	97.6	97.8	97.5	97.8	97.8	97.70	65.0	65.4	65.7	65.8	65.9	65.7	65.70
95.0	95.3	95.1	95.0	95.4	95.3	95.22	60.0	60.0	60.0	59.8	59.6	59.9	59.86
92.5	92.6	92.6	92.7	92.5	92.5	92.58	55.0	55.3	55.2	55.3	55.3	55.1	55.24
90.0	90.3	90.1	90.2	90.0	90.2	90.16	50.0	50.5	50.5	50.6	50.5	50.7	50.56
87.5	87.9	87.8	87.8	87.6	87.9	87.80	45.0	45.1	45.4	45.3	45.3	45.5	45.32
85.0	85.1	85.0	85.2	85.5	85.2	85.20	40.0	40.5	40.4	40.4	40.2	40.6	40.42
82.5	82.9	82.7	82.7	82.5	82.7	82.70	35.0	35.7	35.6	35.5	35.7	35.8	35.66
80.0	80.5	80.4	80.4	80.3	80.4	80.40	30.0	30.9	30.7	30.2	30.9	30.7	30.68
75.0	75.6	75.6	75.6	75.2	75.2	75.44	25.0	25.9	25.9	25.8	25.7	25.8	25.82

Table 4. Argon percentage values of the twenty Argon-air mixtures created for IGU2 sample (readings are obtained by HIGC)

Replicate 1 (IGU2)													
Argon target (%)	1	2	3	4	5	Avg	Argon target (%)	1	2	3	4	5	Avg
100.0	100.0	100.2	100.1	100	100	100.0	70.0	70.2	70	70.1	70.4	70.3	70.20
97.5	97.7	97.8	97.6	97.8	97.5	97.68	65.0	65.4	65.3	65.6	65.6	65.4	65.46
95.0	95.1	95.0	95.1	95.2	95.0	95.08	60.0	60.5	60.0	60.0	60.4	60.3	60.24
92.5	92.1	92.3	92.1	92.4	92.4	92.26	55.0	55.3	55.4	55.3	54.9	55.2	55.22
90.0	89.3	89.5	89.4	89.6	89.6	89.48	50.0	50.5	50.7	50.6	50.7	50.6	50.62
87.5	87.0	87.1	87.2	86.7	86.5	86.90	45.0	46.2	46.0	46.1	45.8	45.8	45.98
85.0	84.2	84.2	84.3	84.3	84.3	84.26	40.0	41.0	40.7	40.6	40.9	40.7	40.78
82.5	82.3	82.2	82.3	82.2	82.2	82.24	35.0	36.2	35.7	35.8	36.1	36.0	35.96
80.0	79.9	79.9	80.0	80.0	79.7	79.90	30.0	31.6	31.2	31.3	30.9	31.0	31.20
75.0	74.9	75.0	75.0	75.0	74.8	74.94	25.0	27.3	27.3	27.4	27.3	27.4	27.34
Replicate 2 (IGU2)													
Argon target (%)	1	2	3	4	5	Avg	Argon target (%)	1	2	3	4	5	Avg
100.0	100.0	99.8	99.9	100.1	100	99.96	70.0	70.2	70.1	70.2	70	70.1	70.12
97.5	97.9	97.8	97.5	97.5	97.6	97.66	65.0	65.3	65.2	65.3	65.2	65.1	65.22
95.0	94.7	94.9	94.9	95.0	94.9	94.88	60.0	60.2	60.2	60.1	60.2	60.0	60.14
92.5	92.7	92.7	92.6	92.7	92.7	92.68	55.0	55.3	55.2	55.3	55.1	55.2	55.22
90.0	90.3	90.2	90.4	90.2	90.2	90.26	50.0	50.5	50.5	50.4	50.5	50.5	50.48
87.5	87.8	87.7	87.7	87.7	87.6	87.70	45.0	45.6	45.6	45.6	45.5	45.6	45.58
85.0	85.2	85.2	85.1	85.4	85.4	85.26	40.0	40.7	40.8	40.6	40.6	40.7	40.68
82.5	82.2	82.3	82.4	82.6	82.5	82.40	35.0	35.8	35.7	35.7	35.8	35.6	35.72
80.0	79.7	79.6	79.8	79.7	79.7	79.70	30.0	31.0	31.0	31.0	30.9	30.8	30.94
75.0	74.8	74.8	74.9	74.9	74.8	74.84	25.0	27.3	27.2	27.4	27.3	27.3	27.30
Replicate 3 (IGU2)													
Argon target (%)	1	2	3	4	5	Avg	Argon target (%)	1	2	3	4	5	Avg
100.0	99.7	99.8	100	99.7	100.1	99.86	70.0	70.3	70.5	70.4	70.3	70.4	70.38
97.5	97.5	97.6	97.6	97.6	97.5	97.56	65.0	65.7	65.5	65.8	65.4	65.4	65.56
95.0	95.0	95.1	9.05	95.2	95.0	95.06	60.0	60.6	60.7	60.5	60.6	60.5	60.58
92.5	92.3	92.5	92.5	92.7	92.5	92.50	55.0	55.8	55.3	55.2	55.3	55.2	55.36
90.0	90.0	90.1	90.0	89.9	90.1	90.02	50.0	50.2	50.3	50.2	50.1	50.4	50.24
87.5	87.6	87.6	87.5	87.6	87.6	87.58	45.0	45.9	45.9	45.8	45.8	45.8	45.84
85.0	85.2	85.1	85.0	85.2	85.0	85.10	40.0	40.7	40.8	40.7	40.9	40.7	40.76
82.5	82.8	82.8	82.7	82.9	83.0	82.84	35.0	36.2	36.1	36.2	36.1	36.0	36.12
80.0	80.5	79.5	80.4	80.3	80.3	80.20	30.0	31.2	31.4	31.2	31.2	31.4	31.28
75.0	75.2	75.4	75.5	75.2	75.5	75.36	25.0	26.5	26.3	26.3	26.4	26.3	26.36

Step 2: Performing UT Measurements on Gas-filled IGUs

Based on the application the UT methodology is categorized into two modes: (i) linear UT (Sasmal et al. 2023; Wu et al. 2023); and (ii) nonlinear UT (Mostavi et al. 2017; Nilsson et al. 2023). In this study, the nonlinear ultrasonic mode is not considered due to its incompatibility with the material properties of the glass-gas system. Nonlinear mode is primarily utilized for heterogeneous materials, such as concrete, where it is mainly used for defect detection (Zhang 2024). Moreover, the comparison between non-contact and contact UT methods demonstrates that the contact method significantly enhances ultrasonic wave transmission through the IGU samples due to the reduction to only two boundaries (i.e., glass-gas boundaries). However, the non-contact method introduces air as an additional boundary, causing acoustic mismatch and impeding wave transmission. The contact method also minimizes losses in ultrasonic wave transmission through the IGU's lite and improves the transmission coefficient of transducers (Butkus et al. 2004).

Therefore, this study employs the linear UT mode using the through-transmission as a contact UT setup, where transducers are positioned on both sides of the IGU samples. UT measurements are performed on the IGU samples to capture different waveforms corresponding to their associated mixture percentages (e.g., 100% Argon, 97.5% Argon, 95% Argon, etc.). The entire process of UT measurements is conducted three times for two IGU samples, resulting in a total of six replicates. For each replicate of the twenty Argon-air mixtures, three waveforms are extracted from each UT measurement for five times, leading to a total of 300 ultrasonic waveforms.

Figure 4 illustrates the UT measurement setup, which employs a PCI-8 data acquisition (DAQ) system and transducers from MISTRAS Group Inc. The R6 transducers, resonant with a peak near 60 kHz, function as both receiver and transmitter. The receiver is linked to a 40 dB preamplifier and then to the PCI-8 DAQ system. For the UT measurements, the transducers are adhered to the center of the IGU using hot glue as a couplant and are taped to the IGU lites to minimize coupling effects and ensure the stability of the transducers during the gas mixture transfer process. The data acquisition parameters are set with an analog filter range of 20–400 kHz and a sampling rate of 1 MHz. A ten-cycle tone burst signal with a 10-V amplitude is used as the excitation signal, with the frequency set to 60 kHz. While the resolution of UT measurement improves with higher frequencies due to the smaller wavelength, penetration through air is significantly limited by wave attenuation. This limitation is particularly critical because of the impedance mismatch between the glass lites and the IGU spacer. The choice of a 60 kHz ultrasonic frequency ensures sufficient wave energy propagation through three interfaces while maintaining adequate sensitivity.

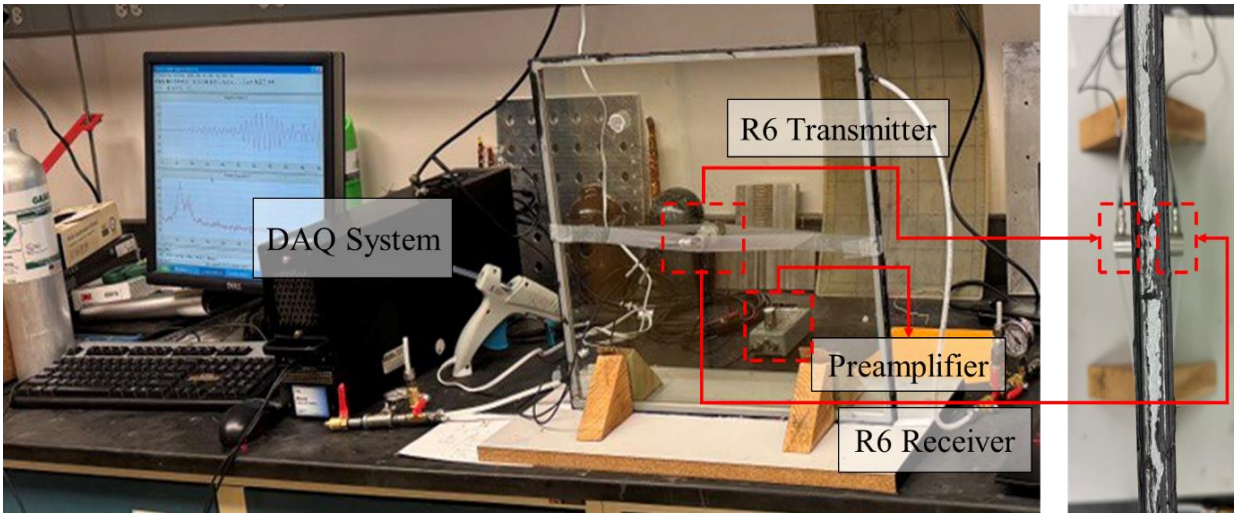

Figure 4. Through-transmission UT experimental setup on the IGU1 using linear UT [Khaleghi et al. 2025]

Step 3: Analyzing Ultrasonic Waveforms

To quantify the Argon concentration within the IGU samples, the UT waveforms for all twenty target mixtures—tested in three replicates for each of the two IGU samples—are analyzed to determine the most effective UT feature for correlating the UT signals with the Argon concentration within the IGU spacer. Typical UT features include ToF, amplitude, energy, and frequency. The Argon concentration within the two lites of an IGU is anticipated to affect the ultrasonic wave speed (i.e., ToF) and the transmission coefficient (i.e., ultrasonic energy). ToF is determined by determining the arrival time of the first ultrasonic signal from the transmitter to the receiver, defined as the time above a predefined threshold. Ultrasonic energy calculation involves analyzing waveforms by converting negative amplitudes to positive (i.e., absolute amplitude values) within a selected time window and then determining the area under the waveform amplitude.

Therefore, UT waveforms demonstrate two key parameters: (1) wave speed, quantified by ToF, and (2) transmission coefficient, quantified by ultrasonic energy. Khaleghi et al. (2025) found that the first UT parameter (i.e., ToF) is insufficient for measuring Argon concentration within IGUs. Although it is expected that higher Argon concentrations would result in longer ToF due to Argon's greater density compared to air, inconsistent ToF readings were observed due to several factors such as temperature fluctuations, material inhomogeneity, surface conditions of the lites, and the substantial acoustic impedance between the lite and the gas mixture. Moreover, the minimal difference in ultrasound velocity between Argon (319 m/s) and air (343 m/s) further complicates the use of ToF as a reliable UT feature. Therefore, attention must be redirected towards the second UT parameter (i.e., ultrasonic energy). Unlike ToF, which primarily depends on wave velocity and becomes harder to measure in signals with low signal-to-noise ratio, ultrasonic energy provides a holistic response of structure including material properties, particularly density, elastic properties and wave dispersion. Ultrasonic energy also captures amplitude and frequency content of the wave as it is based on the cumulative energy under the waveform. This approach over time helps mitigate

the impact of transient fluctuations and noise, resulting in a more robust and consistent feature for waveform analysis. Figure 5 presents the aggregated energy values for each of the twenty Argon-air mixtures, derived from three replicates for each IGU sample. For energy values across all six replicates, refer to Figure S1 in the supplementary materials document. Unlike ToF values, ultrasonic energy exhibits an apparent correlation with Argon concentration, with increased Argon concentrations resulting in higher ultrasonic energy values.

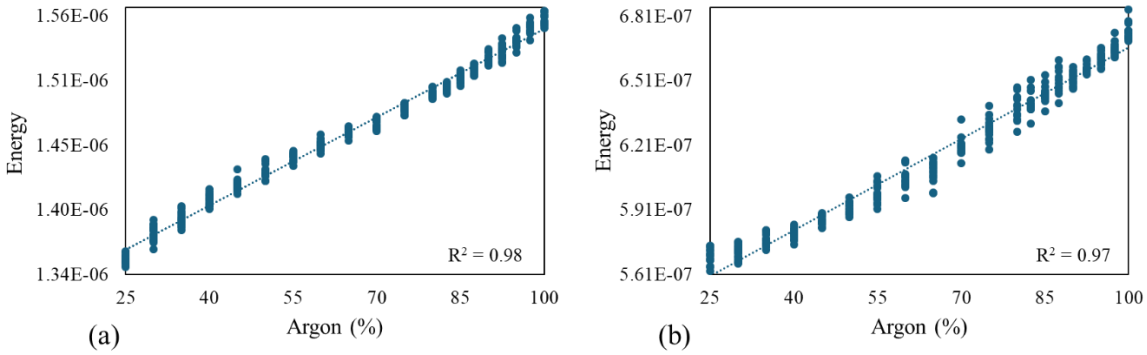

Figure 5. Energy values corresponding to the Argon target mixture for: (a) IGU1; and (b) IGU2

Step 4: Applying Statistical Methods for Argon Quantification

To ensure the accuracy of the Argon concentration measurements, 15 energy values were obtained from the UT waveform analysis for each Argon-air mixture, and the average was taken to determine the corresponding Argon concentration percentage. Data points deviating more than ±1% from the average were excluded as outliers. This criterion was chosen because the energy values were very close to each other, making ±1% a reasonable threshold. Excluding outliers ensures the integrity and precision of the measurements, while minimizing any potential experimental inconsistencies or noise that might affect the results. After removing outliers from the raw dataset (Figure 5), the ultrasonic energy values are normalized using the natural logarithm (ln) transformation to improve the accuracy of converting ultrasonic energy values into Argon concentration values. Finally, the correlation between Argon concentration and ultrasonic energy values is represented in Equation 1.

$$Argon\ (\%) \sim \ln\left(\int_{t_1}^{t_2} |time\ dependent\ amplitude| dt\right) \quad (1)$$

$Argon\ (\%)$ represents the concentration of Argon for each targeted Argon-air mixture, t_1 and t_2 denote the start and end duration of the time window used to compute the ultrasonic energy value, and $|time\ dependent\ amplitude|$ refers to the absolute value of signal amplitude generated by the transmitter and captured by the receiver during UT measurements.

Regression analysis is conducted for the ultrasonic energy dataset due to the minimal differences between ultrasonic energy values for each Argon-air mixture. To derive Argon concentration from the energy values, several regression models are applied, including linear regression, k-nearest neighbors, random forest regression, gradient boosting regression, support vector regression, and multilayer perceptron. All models use 80% of the data points for training and 20% for testing. R-squared (R^2), mean absolute error (MAE), and mean squared error (MSE) are used to evaluate the

performance of the models on the test set. Equations 2, 3, and 4 define these indicators, respectively.

$$R^2 = 1 - \left[\sum_{n=1}^{N=20}\left(Ar_{A,n} - Ar_{M,n}\right)^2 / \sum_{n=1}^{N=20}\left(Ar_{A,n} - \overline{Ar_A}\right)^2\right] \quad (2)$$

$$MAE = \frac{1}{N}\sum_{n=1}^{N=20}\left|Ar_{A,n} - Ar_{M,n}\right| \quad (3)$$

$$MSE = \frac{1}{N}\sum_{n=1}^{N=20}\left(Ar_{A,n} - Ar_{M,n}\right)^2 \quad (4)$$

$Ar_{A,n}$ is the actual value of the Argon concentration, $Ar_{M,n}$ is the measured value of the Argon concentration with the proposed UT methodology, and $\overline{Ar_A}$ is the actual average value of the Argon concentration. N is the total number of the target Argon-air mixtures and n is the mixture number corresponding to each Argon-air mixture (see Table 2). All of the aforementioned regression models achieved R^2 values exceeding 0.97 and MAE less than 3. However, linear regression outperformed the others due to its great interpretability and explainability, which also mitigates the risk of overfitting.

Figure 6 depicts the aggregated actual (i.e., target Argon-air mixtures) and predicted Argon concentration values from the six replicates for the two IGU samples, along with their corresponding transformed ultrasonic energy values derived from the UT measurements on the twenty Argon-air mixtures. For trends across all six replicates, refer to Figure S2 in the supplementary materials document. Based on the target Argon-air mixtures, R^2, MAE, and MSE metric values for each replicate are also presented in Figure 6. The results demonstrate that the proposed UT methodology exhibits exceptional accuracy in measuring Argon concentration within IGUs. This is evidenced by an R^2 value of 0.99, MAE of less than 0.17, and MSE of less than 0.09 for the two IGU samples.

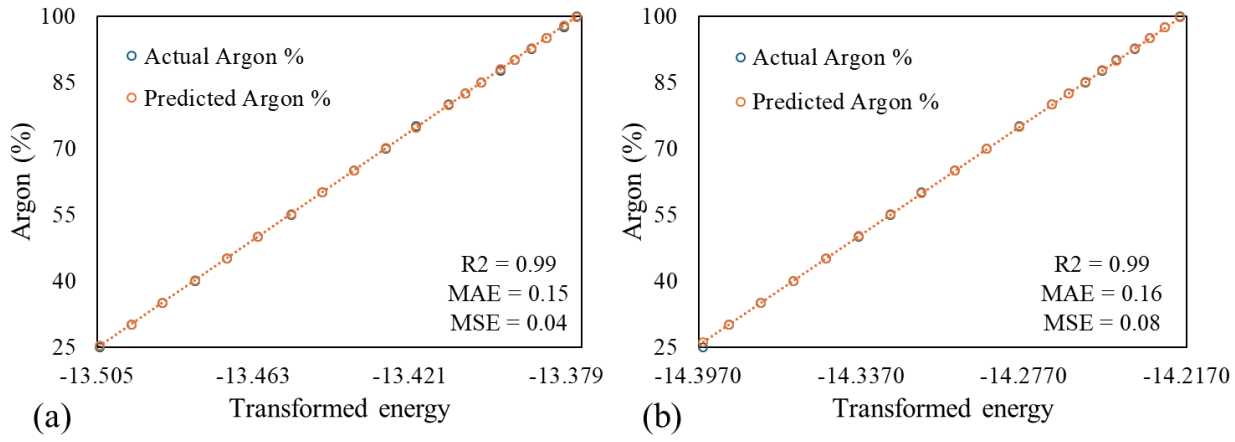

Figure 6. Argon concentration corresponding to the transformed ultrasonic energy values for: (a) IGU1; and (b) IGU2

Section 2- Numerical Analysis

To validate the UT measurements, the experiment components (e.g., the gas-filled IGU samples and R6 transducers) are modeled and analyzed using COMSOL Multiphysics®. Then the models enable a comparison between the experimental UT signals and the corresponding numerical simulations to validate the accuracy and consistency of the UT measurements. This section includes Step 5 and Step 6 as explained in detail below.

Step 5: Implementing Numerical Model

Figure 7 presents the finite element model setting simulating the IGU2 sample under UT. The model features a sandwich configuration, with glass as the outer layers and Argon-air mixture as the inner layer. To simulate the UT setup, two circular regions were defined at the center of the glass surfaces, representing R6 transducers with identical dimensions to those used in experiment. The Hanning window excitation signal with frequency of 60 kHz, was generated in MATLAB to align with the experiment (Figure 7a). The tetrahedral mesh elements were used with the minimum size of 0.0063 m, to ensure the convergence of the model (Figure 7b).

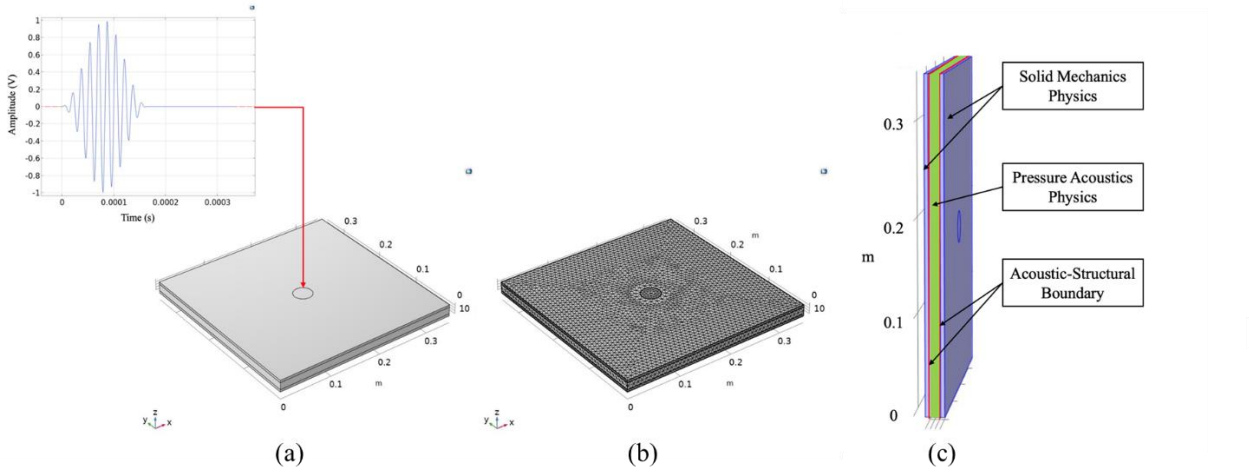

Figure 7. COMSOL Multiphysics® model settings: (a) IGU2 sample and R6 transducer boundary conditions; (b) mesh model; and (c) multi-physics interfaces

According to Figure 7c, the multi-physics model includes two interfaces: The first interface is solid mechanics physics, which models the mechanical behavior of the glass layers. This interface calculates structural deformations and stresses in the glass when subjected to external forces or internal pressures, simulating how the glass responds to ultrasonic waves propagating through the glass layers. The second interface is pressure acoustics physics, which models the propagation of acoustic waves in the Argon-air mixture. This interface captures variations in the acoustic pressure field, showing how the gas medium reacts to the transmission of ultrasonic waves propagating through the gas mixture. To simulate the interaction between these two physic interfaces, acoustic-structural boundary conditions were defined to couple the pressure acoustics and solid mechanics physics. They enable interaction between the Argon-air mixture and the glass layers, accounting for how ultrasonic pressure waves transmit within two different interfaces.

To simulate how the various Argon-air mixtures affect the UT signals, the different densities of the Argon-air mixture due to the Argon-air mixture proportion were determined. To calculate the gas

mixture density, the molar mass for each gas mixture is initially determined based on Equation 5, followed by the application of the ideal gas law (see Equation 6).

$$M_{Mix} = (X_{Air}.M_{Air}) + (X_{Ar}.M_{Ar}) \quad (5)$$

$$\rho_{Mix} = \frac{P.M_{Mix}}{R.T} \quad (6)$$

X_{Air} and X_{Ar} refer to the volume of Air and Argon in each gas mixture in liters. M_{Air} and M_{Ar} refer to the molar mass of Air and Argon, which are 28.97 g/mol and 39.95 g/mol, respectively. R refers to the ideal gas constant, which is 0.0821 L.amt/mol.K. Also, P is the pressure of the gas mixture, and T is temperature, both of which are considered under ambient laboratory conditions (101325 Pa and 297.15 K). Table 5 presents the molar mass and corresponding density values for each Argon-air mixture.

Table 5. Molar mass and density values for created Argon-air mixtures

Mixture No.	**1**	**2**	**3**	**4**	**5**	**6**	**7**	**8**	**9**	**10**
Argon (%)	100	97.5	95	92.5	90	87.5	85	82.5	80	75
M_{Mix}	39.94	39.67	39.39	39.12	38.84	38.57	38.29	38.02	37.75	37.20
ρ_{Mix}	1.637	1.626	1.615	1.603	1.592	1.581	1.570	1.558	1.547	1.525
Mixture No.	**11**	**12**	**13**	**14**	**15**	**16**	**17**	**18**	**19**	**20**
Argon (%)	70	65	60	55	50	45	40	35	30	25
M_{Mix}	36.65	36.10	35.55	35.00	34.46	33.91	33.36	32.81	32.26	31.71
ρ_{Mix}	1.502	1.480	1.457	1.435	1.412	1.390	1.367	1.345	1.322	1.300

With the densities for each Argon-air mixture, the model then undergoes time-dependent computation, with excitation signals transmitted from one lite and received from the opposite lite of the IGU for subsequent waveform analysis. Figure 8 illustrates the sequence of how the acoustic wave propagates through the gas mixture. The progression over time demonstrates the initial wave interaction with the glass layers and its subsequent travel through the gas medium.

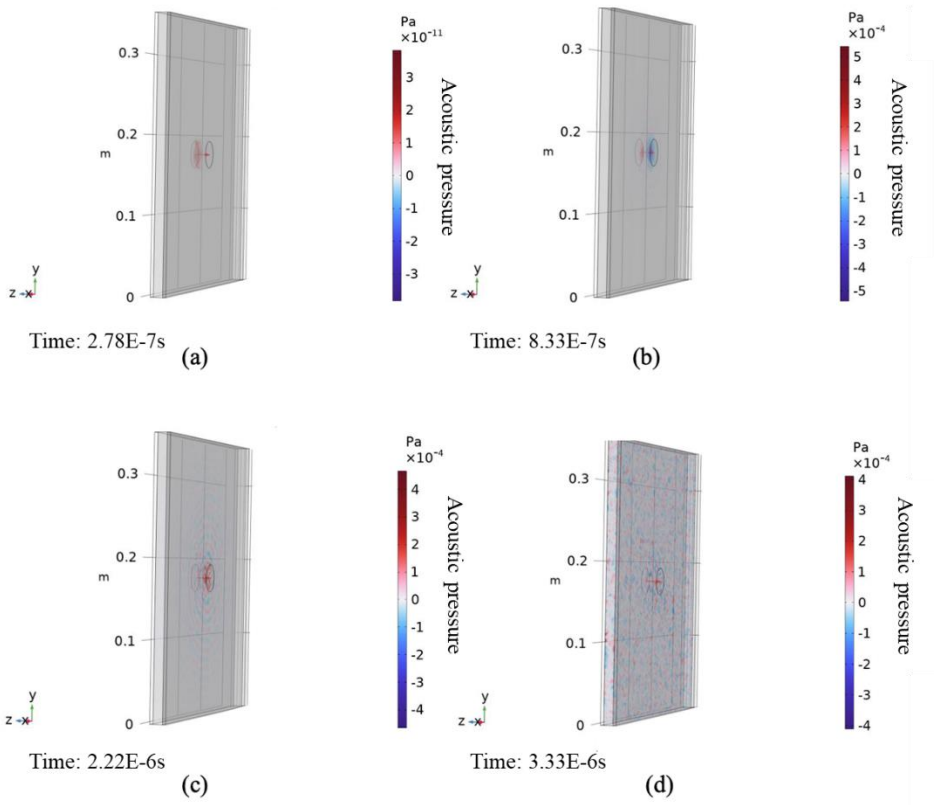

Figure 8. Wave propagation through gas mixture over time.

This simulation allows for the observation of the time-dependent stress distribution across the entire glass-gas system. For instance, Figure 9 shows the sequence of images captured at the different progression times of ultrasonic waves which represent the propagation of UT signals and stress distribution through the IGU (i.e., glass lites and gas mixture). The UT signal originates from the transducer at the central point, creating a uniform circular wave pattern within the IGU. This wave propagates outward in all directions, maintaining the regular pattern as it spreads (Figure 9a). The UT signal propagation continues by interacting with the glass and gas mixture of the IGU (Figure 9b). The interaction causes reflections and refractions, which can be seen in the following images where the wave patterns start to show distortions and more complex patterns. As the UT signal continues to propagate, it begins to meet the boundaries of the IGU, (i.e., the edges of the IGU). These boundaries create variations in wave propagation. This interaction starts to change the initially uniform circular pattern, creating more complex waveforms as the waves begin to bounce back and interact with each other (Figure 9c). This interaction with the edges of the IGU introduces multiple reflections, leading to increasingly complex wave patterns (Figure 9d). The wave patterns, influenced by ongoing reflections and interactions, form a network of stress lines throughout the IGU. This denser stress distribution indicates that the UT signals are continuously interacting with the IGU boundaries and gas mixtures, leading to a more uniform but complicated pattern of stress (Figure 9e). The UT signal has now fully propagated through the IGU, with the wave patterns stabilizing with lower stresses but still showing a high level of complexity. This has

resulted in a stress distribution that extends throughout the IGU, reflecting the interactions between the UT signal and the IGU (Figure 9f).

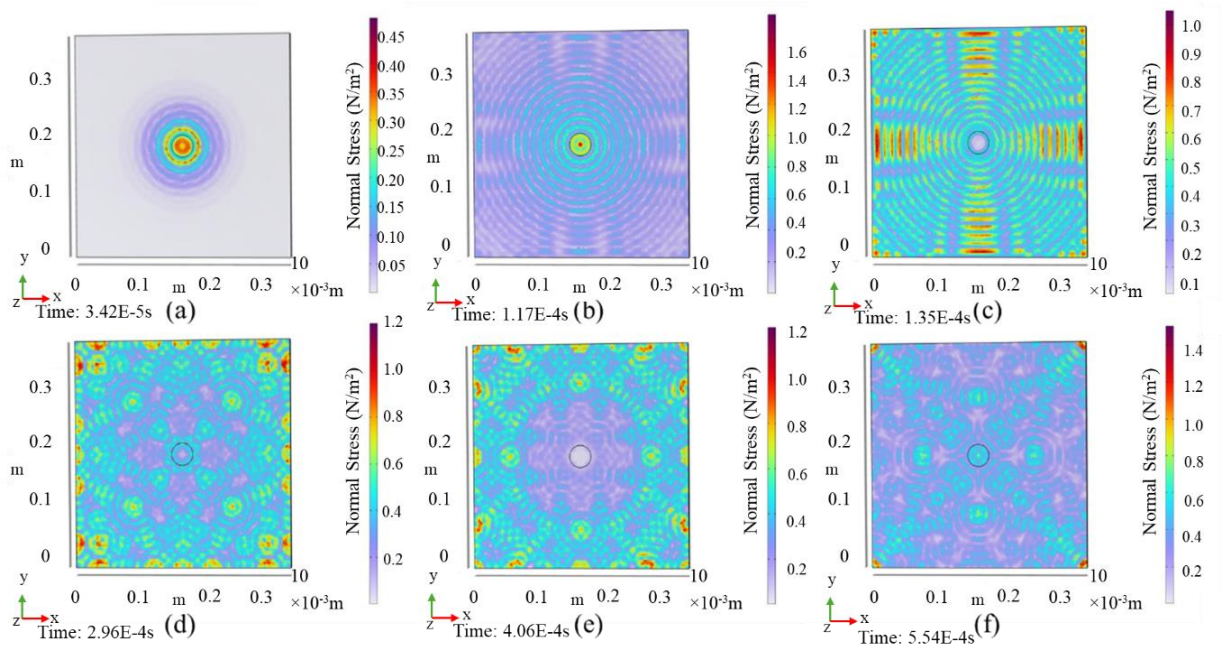

Figure 9. Time-dependent stress distribution during the UT signal propagation through IGU1 sample

Step 6: Validating Experiment by Numerical Model

UT signals generated by the numerical model for four selected Argon-air mixtures (100% Argon, 80% Argon, 50% Argon, and 25% Argon) are plotted in Figure 10 and Figure 11 for IGU1 and IGU2 samples, respectively. To enhance the recognition of the ToF, the first 200 µs is magnified. The results demonstrate that the waveform patterns and the ToF in the numerical model are similar to the experimental measurements, with minor differences attributed to the coupling effect used in the experiment. Moreover, as shown in Figure 10 and Figure 11, the ToF for IGU2, which is thicker, is longer compared to IGU1 due to the increased propagation distance. For the analysis of UT waveforms, the energy is determined within the time windows of 59 µs to 180 µs for IGU1 and 65 µs to 135 µs for IGU2. These time windows are selected based on the expected ToFs, with the first arrival signals occurring within the initial 10 cycles. Beyond 180 µs for IGU1 and 135 µs for IGU2, UT signals start to exhibit new arrivals due to reverberations from glass boundaries, causing inconsistencies that hinder accurate waveform analysis. Therefore, other parts of the UT signals are disregarded in the waveform analysis.

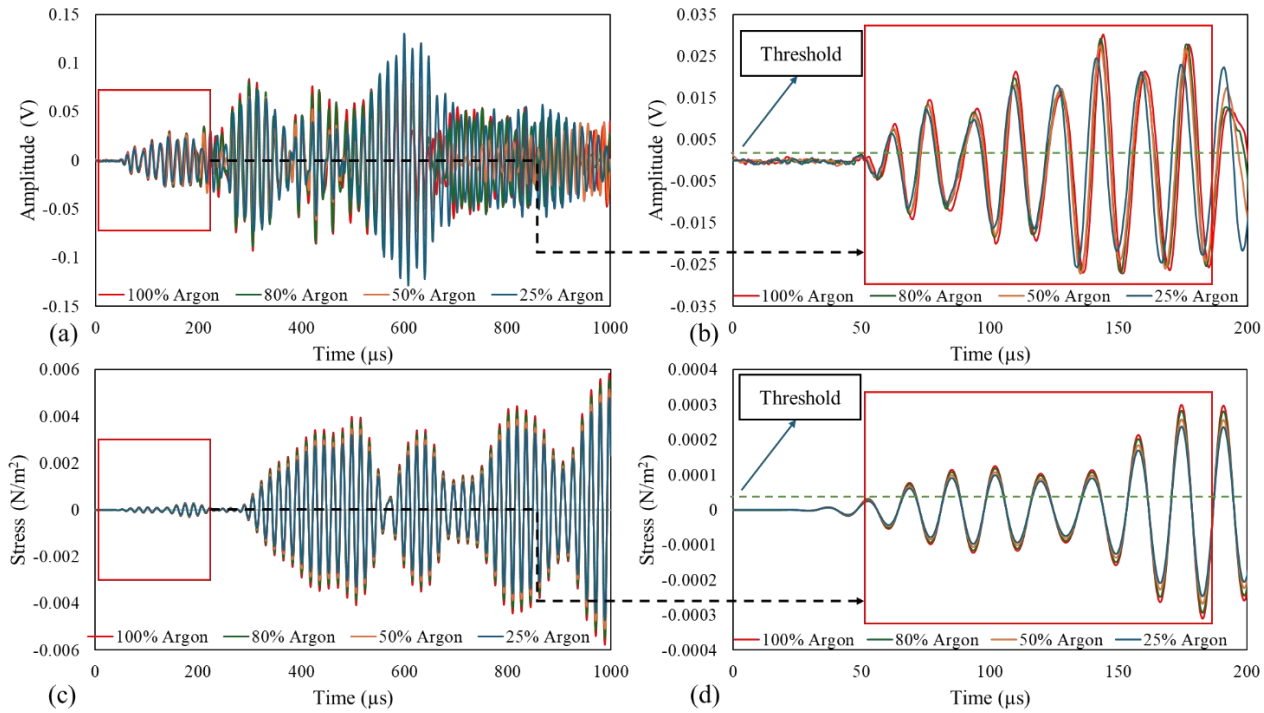

Figure 10. Sample of UT signals for IGU1: (a) entire UT signals from experiment; (b) processed time window of UT signals [59 μs – 180 μs] from the experiment; (c) entire UT signals from numerical model; (d) processed time window of UT signals [59 μs – 180 μs] from numerical model

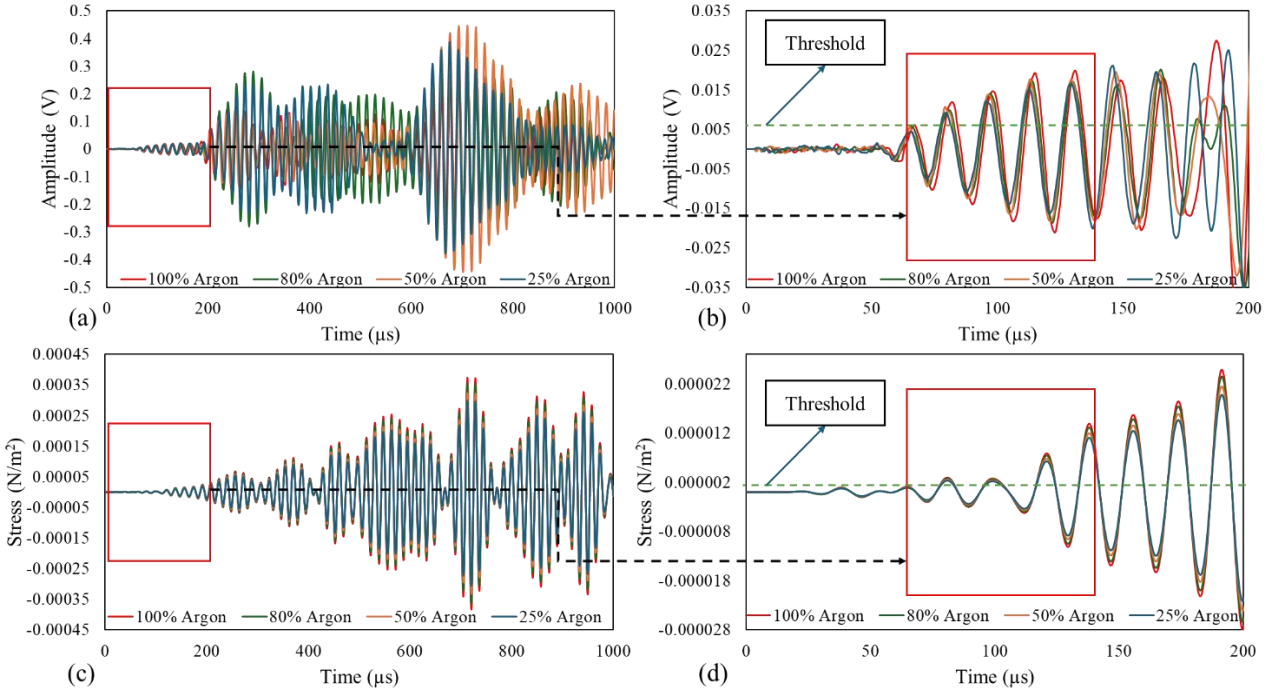

Figure 11. Sample of UT signals for IGU2: (a) entire UT signals from experiment; (b) processed time window of UT signals [65 μs – 135 μs] from the experiment; (c) entire UT signals from

numerical model; (d) processed time window of UT signals [65 µs – 135 µs] from numerical model

Energy values were then extracted from UT signals for further analysis. Figure 12 shows a rising trend in the energy values as the Argon percentage in an Argon-air mixture increases for both IGU samples. This trend is consistent with the experimental results presented in Figure 5 and Figure 6. Argon's higher density, compared to air, enhances its ability to transmit ultrasonic waves with less energy loss due to its lower absorption and scattering characteristics. Moreover, Argon's higher acoustic impedance improves wave transmission efficiency, leading to greater energy preservation. The energy values for the thicker IGU2 are lower compared to IGU1. The energy transmitted through a material (i.e., the glass-gas system in this case) depends on the impedance mismatch between the gas mixture and the glass. Generally, the greater the thickness of the glass, the more potential there is for wave reflection at each interface, causing some energy to be reflected back each time a wave hits a boundary. Moreover, as ultrasonic waves travel through a longer medium, they lose energy due to absorption, which converts part of the wave energy into heat within the medium. Thicker glass results in a longer path within the material, increasing absorption and reducing the energy that can pass through. Therefore, these findings validate the consistency between experimental results and numerical outcomes, demonstrating that the energy values vary with the IGU type (i.e., the thickness of the glass lites and spacer). Since there are relatively few variations in IGUs' lite and spacer thickness, it is feasible to develop a calibration equation that applies to different IGU designs. This can be achieved through a one-time experimental calibration process, involving the generation of Argon-air mixtures and quantifying the Argon concentration for each IGU design with different lite and spacer thicknesses.

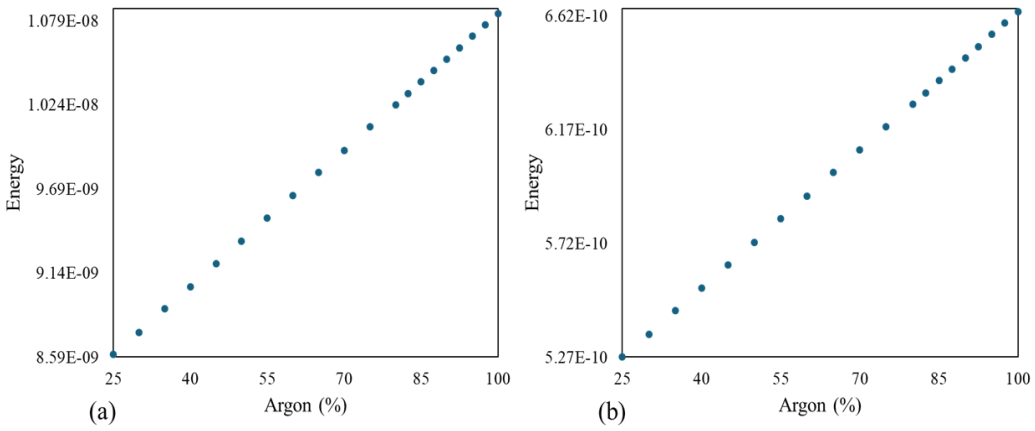

Figure 12. Energy values corresponding to the Argon-air target mixtures from the numerical model: (a) IGU1; (b) IGU2

Section 3- Comparison Analysis

This section presents the findings regarding Argon concentration values obtained from the three different methodologies employed in this study. Argon concentrations are also measured using the gas analyzer (HIGC) and the commercial device (SES) for each target Argon-air mixture while UT

signals are generated for the subsequent UT waveform analysis (Step 7). After obtaining Argon concentration measurements from all three methodologies, these readings are compared to evaluate the performance of each methodology (Step 8). The performance of the three methodologies is assessed through the Mean Absolute Error (MAE), Mean Squared Error (MSE) metrics, and error bars, providing a comprehensive evaluation of their performance.

Step 7: Measuring Argon Concentration Values with Commercial Device (SES) and Gas Analyzer (HIGC)

In this study, the Argon concentration within the IGU samples, quantified by the proposed UT methodology, is compared with two other methodologies: (1) commercial device using spark emission spectroscopy method (SES) and (2) Helantec ISO-Gas-Control (HIGC). SES is considered as the non-destructive approach, while HIGC is considered as the destructive approach. Both SES and HIGC measurements comply with ASTM E2649-20 and the manufacturer's manual, including specifications such as the number of measurements, laboratory temperature, the intensity of lights during the experiment, and the use of low-e coating and uncoated lites for IGU samples.

On the edge of the IGU samples (i.e., close to the inlet and outlet tubes), SES is positioned to take Argon concentration readings within the spacer of the IGU samples. From each measurement location and each Argon-air mixture using SES, five readings are taken, with the three closest to the target mixtures recorded, resulting in six readings per Argon-air mixture. Moreover, for HIGC, five readings are taken by extracting a gas sample from the outlet of the IGU samples, which are then averaged. It is important to note that the Argon concentration measurements with SES and HIGC are performed concurrently with the UT experiments, meaning the readings correspond to the same gas mixture used for generating the UT waveforms.

Step 8: Comparing the Proposed UT Methodology with the Commercial device (SES) and the Gas Analyzer (HIGC)

Figure 14 explains that the error bar of the proposed UT methodology has significantly lower error ranges compared to the SES and HIGC devices, evidenced by the reduced size of the error bar in the UT methodology. For more detailed results on MAE and MSE values, as well as error bars for the six replicates across the three methodologies, refer to Table S1 and Figure S3 in the supplementary materials document, respectively. Table 6 provides the average measurement values of Argon concentration for all six measurements across the three methodologies, along with the respective 95% confidence intervals. For the measurement readings of all six replicates across the three methodologies, refer to Table S2 and Table S3 in the supplementary materials document. The combined results from IGU1 and IGU2 samples for all replicates indicate that the error of the proposed UT methodology, SES, and HIGC is 0.14, 2.31, and 0.33, respectively.

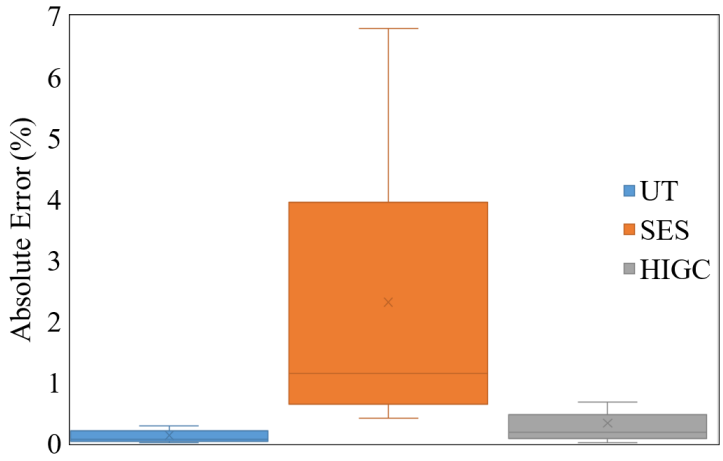

Figure 14. Absolute error bars for UT, SES, and HIGC methodologies

Table 6. Comparison of Argon concentration measurements, including 95% confidence intervals (CI), obtained by the proposed UT methodology, commercial device (SES), and gas analyzer (HIGC)

Argon target (%)	**UT**		**SES**		**HIGC**	
	Avg	95% CI	Avg	95% CI	Avg	95% CI
100.0	99.75	[99.67, 99.83]	99.36	[98.83, 99.88]	99.87	[99.68 100.07]
97.5	97.65	[97.35, 97.96]	97.94	[97.71, 98.17]	97.40	[97.06 97.74]
95.0	95.05	[94.99, 95.11]	95.65	[95.13, 96.16]	95.02	[94.78 95.27]
92.5	92.72	[92.56, 92.89]	92.92	[92.27, 93.56]	92.46	[92.33 92.59]
90.0	90.03	[89.79, 90.26]	90.47	[89.45, 91.49]	90.28	[89.42 91.14]
87.5	87.78	[87.66, 87.90]	88.31	[87.17, 89.45]	87.39	[86.86 87.91]
85.0	85.01	[84.79, 85.22]	86.14	[84.51, 87.78]	84.87	[84.32 85.42]
82.5	82.44	[82.23, 82.65]	83.38	[82.25, 84.52]	82.46	[82.20 82.72]
80.0	79.88	[79.68, 80.08]	81.25	[80.21, 82.29]	80.01	[79.65 80.36]
75.0	74.76	[74.64, 74.89]	76.14	[75.01, 77.27]	75.07	[74.48 75.65]
70.0	69.93	[69.79, 70.07]	72.99	[71.82, 74.16]	70.16	[69.54 70.79]
65.0	64.94	[64.72, 65.15]	70.25	[68.92, 71.58]	65.43	[65.03 65.82]
60.0	59.93	[59.74, 60.12]	65.03	[62.57, 67.49]	60.19	[59.79 60.60]
55.0	55.08	[54.86, 55.29]	58.90	[56.85, 60.95]	55.28	[54.80 55.76]
50.0	50.01	[49.80, 50.21]	53.52	[51.28, 55.77]	50.25	[49.87 50.63]
45.0	45.03	[44.88, 45.18]	48.99	[47.74, 50.25]	45.48	[45.06 45.90]
40.0	40.04	[39.95, 40.13]	46.80	[45.64, 47.95]	40.54	[40.07 41.01]
35.0	35.02	[34.74, 35.31]			35.67	[35.16 36.19]
30.0	30.12	[29.87, 30.36]			31.15	[30.71 31.60]
25.0	25.75	[25.06, 26.45]			26.59	[25.90 27.28]

Unlike SES and HIGC, the UT methodology's ability to accurately capture the Argon concentration does not decline at any concentrations, ensuring consistent performance across the full range of Argon-air mixtures. Another critical advantage is that the UT approach can be integrated into the existing manufacturing process of IGUs, as well as allowing for in-situ measurements without the need for extracting gas samples or disrupting the system. This capability significantly improves

the detection of gas leakage defects that may arise due to natural climatic conditions, as well as issues related during the manufacturing process. The proposed UT methodology offers significant advantages in accessibility, affordability, and ease of implementation. Unlike the SES and HIGC, which require specialized equipment, the UT methodology is straightforward to use and more cost-efficient, providing a practical solution without compromising accuracy. This makes it a highly viable alternative for measuring Argon concentration in IGU samples, suitable for both research and industry applications.

Future Work

Future work will aim to extend this methodology to quantify not only Argon but also other heavy inter gases such as Krypton and Xenon gases by testing a broad range of IGU samples with diverse designs and materials to develop a more generalized and accessible measurement approach. Extensive studies will be conducted for accurately quantifying heavy inert gases through numerical simulations. While experimental and simulation results show consistent trends, discrepancies in ultrasonic energy values remain due to experimental variables such as pressure between transducers and IGU lites, temperature fluctuations, and other noise sources. To address these, experiments on various IGU types with different lite and spacer thicknesses will be conducted to create a comprehensive dataset. Moreover, IGU age must be considered as one of the main factors influencing Argon concentration due to aging. This dataset will enable numerical modeling to quantify inert gases based on IGU specifications, environmental conditions, and IGU age, eliminating the need for physical experiments. Additionally, future research will explore the development of a leakage detection tool using the UT methodology to identify and monitor Argon and other inert gas leakage from IGUs under simulated conditions. Advancing this methodology will reduce the need for UT measurements for each IGU design, saving time and costs, while contributing to the development of energy-efficient IGUs and enhancing sustainability needs.

Conclusion

This study introduces a non-destructive ultrasonic testing (UT) methodology as a reliable and accurate means of quantifying Argon concentration within IGUs. The proposed UT methodology is tested using two IGU samples filled with twenty different Argon-air mixtures with Argon concentrations ranging from 25% to 100% in three replicates. The experiments are carried out in linear UT mode using a through-transmission setup. UT signals were analyzed to identify the transmission coefficient (i.e., ultrasonic energy) as the most effective metric for Argon quantification within IGUs. Moreover, numerical models are developed using COMSOL Multiphysics® to validate the experimental results. The findings indicate that the proposed UT methodology not only aligns with the numerical models but also outperforms two market-available devices that utilize the Spark Emission Spectroscopy (SES) method as a non-destructive approach and a gas analyzer, Helantec ISO-GAS-Control (HIGC), used as a destructive method. The results of the proposed methodology are reflected by an R-squared (R^2) value of 0.99, a mean absolute error (MAE) of 0.13, and a mean squared error (MSE) of 0.045. Moreover, when averaging the Argon concentration measurements across all three replicates from the two IGU samples, the error rates for the UT methodology, SES, and HIGC are found to be 0.13, 2.31, and 0.33, respectively. This study establishes the proposed UT methodology as a non-destructive, accurate, and rapid tool,

serving as a practical solution for on-site inspections and as a quality control measure during the manufacturing, maintenance, and operational phases of IGUs. Moreover, the UT methodology enables timely detection of Argon gas leakage, helping to mitigate critical issues such as reduced thermal performance, compromised moisture resistance, and diminished sound-blocking capabilities.

Acknowledgment

The authors of this study sincerely acknowledge Cardinal Glass Industries for their in-kind contribution to this research by providing one of the IGU samples (IGU2) used in the study.

References

Abraham, E., V. Cherpak, B. Senyuk, J. B. ten Hove, T. Lee, Q. Liu, and I. I. Smalyukh. 2023. "Highly transparent silanized cellulose aerogels for boosting energy efficiency of glazing in buildings." *Nat Energy*, 8 (4): 381–396. Nature Publishing Group. https://doi.org/10.1038/s41560-023-01226-7.

ASTM E2649-20; Standard Test Method for Determining Argon Concentration in Sealed Insulating Glass Units Using Spark Emission Spectroscopy

"Argon Analyzer | Leak 0-100% | USA NIST Calibration." 2024. Forensics Detect. Accessed July 03, 2024. https://www.forensicsdetectors.com/products/argon-analyzer-leak-0-100-usa-nist-calibration.

Asphaug, S. K., B. P. Jelle, L. Gullbrekken, and S. Uvsløkk. 2016. "Accelerated ageing and durability of double-glazed sealed insulating window panes and impact on heating demand in buildings." *Energy and Buildings*, 116: 395–402. https://doi.org/10.1016/j.enbuild.2016.01.015.

Bizoňová, S., and M. Bagoňa. 2019. "Gas filling in glass system." *International Review of Applied Sciences and Engineering*, 10 (1): 43–50. Akadémiai Kiadó. https://doi.org/10.1556/1848.2019.0007.

Bliūdžius, R., K. Miškinis, V. Buhagiar, and K. Banionis. 2022. "Sound Insulation of Façade Element with Triple IGU." *Buildings*, 12 (8): 1239. Multidisciplinary Digital Publishing Institute. https://doi.org/10.3390/buildings12081239.

Butkus, J., A. Vladišauskas, and L. Jakevičius. 2004. "The use of ultrasound for investigation of glazing units." *Ultragarsas / Ultrasound*, 51 (2): 7–12.

Cramers, C.A., Janssen, H.G., van Deursen, M.M. and Leclercq, P.A., 1999. High-speed gas chromatography: an overview of various concepts. Journal of chromatography A, 856(1-2), pp.315-329.

Cho, K., D. Cho, B. Koo, and Y. Yun. 2023. "Thermal Performance Analysis of Windows, Based on Argon Gas Percentages between Window Glasses." *Buildings*, 13 (12): 2935. Multidisciplinary Digital Publishing Institute. https://doi.org/10.3390/buildings13122935.

Cuce, E., and S. B. Riffat. 2015. “A state-of-the-art review on innovative glazing technologies.” *Renewable and Sustainable Energy Reviews*, 41: 695–714. https://doi.org/10.1016/j.rser.2014.08.084.

El-Darwish, I., and M. Gomaa. 2017. “Retrofitting strategy for building envelopes to achieve energy efficiency.” *Alexandria Engineering Journal*, 56 (4): 579–589. https://doi.org/10.1016/j.aej.2017.05.011.

EN 1279-3: Glass in building: insulating glass units—part 3: long term test method and requirements for gas leakage rate and for gas concentration tolerances. European Standard (2018)

Ghazi Wakili, K., W. Raedle, A. Krammer, A. Uehlinger, A. Schüler, and Th. Stöckli. 2021. “Ug-value and edge heat loss of triple glazed insulating glass units:A comparison between measured and declared values.” *Journal of Building Engineering*, 44: 103031. https://doi.org/10.1016/j.jobe.2021.103031.

Glora, M., G. Reichenauer, and J. Fricke. 1999. “Non-destructive determination of the rare-gas content of highly insulating window systems.” *Meas. Sci. Technol.*, 10 (7): 592. https://doi.org/10.1088/0957-0233/10/7/304.

Gustavsen, A., B. P. Jelle, D. Arasteh, and C. Kohler. 2007. *State-of-the-Art Highly Insulating Window Frames - Research and Market Review*. LBNL-1133E, 941673.

Haglin, D., “Gas Fill 101: Gas fill options for IGUs.” 2021. Accessed July 3, 2024. https://www.windowanddoor.com/article/gas-fill-101-gas-fill-options-igus.

“Helantec ISO Gas Control.” (HIGC) 2024. *Integr. Autom. Syst.* Accessed April 2, 2024. https://iasmachinery.com/helantec-ig-filling-and-gas-testing-systems/helantec-iso-gas-control/. User Manual

Hoseini, M. R., X. Wang, and M. J. Zuo. 2012. “Estimating ultrasonic time of flight using envelope and quasi maximum likelihood method for damage detection and assessment.” *Measurement*, 45 (8): 2072–2080. https://doi.org/10.1016/j.measurement.2012.05.008.

Jedrusyna, A., and A. Noga. 2016. “Acoustic detector of argon content in air-argon mixture.” *Advanced Mechatronics Solutions*, R. Jabłoński and T. Brezina, eds., 329–334. Cham: Springer International Publishing.

Jelle, B. P., A. Hynd, A. Gustavsen, D. Arasteh, H. Goudey, and R. Hart. 2012. “Fenestration of today and tomorrow: A state-of-the-art review and future research opportunities.” *Solar Energy Materials and Solar Cells*, 96: 1–28. https://doi.org/10.1016/j.solmat.2011.08.010.

Khaleghi, H., Ozevin, D., and Karatas, A., 2025. Non-Destructive Argon Concentration Assessment within Insulating Glass Units (IGUs) using Ultrasonic Technique. Journal of Architectural Engineering (Under Review) https://doi.org/10.48550/arXiv.2501.04804

Kim, H., and J. Kim. 2019. “A Case-Based Reasoning Model for Retrieving Window Replacement Costs through Industry Foundation Class.” *Applied Sciences*, 9 (22): 4728. Multidisciplinary Digital Publishing Institute. https://doi.org/10.3390/app9224728.

Knorr, M. D., J. Wieser, G. Geertz, S. Buddenberg, M. Oechsner, and W. Wittwer. 2016. “Gas loss of insulating glass units under load: internal pressure controlled permeation test.” *Glass Struct Eng*, 1 (1): 289–299. https://doi.org/10.1007/s40940-016-0026-1.

Lasa, J., P. Mochalski, and E. Łokas. 2002. “Determination of argon in air and water.” *Chemia Analityczna*, 47: 839–845.

Lee, H.S., Choi, G.S., Ahn, H.S. and Kang, J.S., 2021. Development of high insulation frame to improve the insulation performance of windows. J. Korean Soc. Living Environ. Syst, 28, pp.362-368.

Likins-White, M., R. C. Tenent, and Z. (John) Zhai. 2023. “Degradation of Insulating Glass Units: Thermal Performance, Measurements and Energy Impacts.” *Buildings*, 13 (2): 551. Multidisciplinary Digital Publishing Institute. https://doi.org/10.3390/buildings13020551.

Lolli, N., and I. Andresen. 2016. “Aerogel vs. argon insulation in windows: A greenhouse gas emissions analysis.” *Building and Environment*, 101: 64–76. https://doi.org/10.1016/j.buildenv.2016.03.001.

Miskinis, K., V. Dikavicius, R. Bliudzius, and K. Banionis. 2015. “Comparison of sound insulation of windows with double glass units.” *Applied Acoustics*, 92: 42–46. https://doi.org/10.1016/j.apacoust.2015.01.007.

Mostavi, A., M. Kabir, and D. Ozevin. 2017. “The integration of superlattices and immersion nonlinear ultrasonics to enhance damage detection threshold.” *Applied Physics Letters*, 111 (20): 201905. https://doi.org/10.1063/1.5007771.

NPR-CEN-ISO: energy performance of buildings—thermal, solar and daylight properties of building components and elements—part 2: explanation and justification (ISO/TR 52022-2:2017). European Committee for standardization (2012)

van Nieuwenhuijzen, E. J., J. I. A. Tetteroo, M. van de Vliet, and E. Melet. 2023. “In situ detection of product age and argon concentration as measure of the re-use potential of insulating glass units in buildings.” *Glass Struct Eng*, 8 (2): 211–233. https://doi.org/10.1007/s40940-023-00225-0.

Nilsson, M., E. Huttunen-Saarivirta, E. Bohner, and M. Ferreira. 2023. “Non-destructive evaluation of corrosion in steel liner plates embedded in concrete using nonlinear ultrasonics.” *Construction and Building Materials*, 408: 133691. https://doi.org/10.1016/j.conbuildmat.2023.133691.

Papaefthimiou, S., E. Syrrakou, and P. Yianoulis. 2006. “Energy performance assessment of an electrochromic window.” *Thin Solid Films*, Selected Papers from the 5th International Conference on Coatings on Glass (ICCG5)- Advanced Coatings on Glass and Plastics for Large-Area or High-Volume Products, 502 (1): 257–264. https://doi.org/10.1016/j.tsf.2005.07.294.

Peng, J., D. C. Curcija, A. Thanachareonkit, E. S. Lee, H. Goudey, J. Jonsson, and S. E. Selkowitz. 2021. “Comparative study on the overall energy performance between photovoltaic and Low-E insulated glass units.” *Solar Energy*, 214: 443–456. https://doi.org/10.1016/j.solener.2020.12.006.

Rasmussen, B. and Gerretsen, E., 2014. Proposal for an acoustic classification scheme for housing. In COST Action TU0901–Building acoustics throughout Europe. Volume 1: Towards a common framework in building acoustics throughout Europe (pp. 81-100). DiScript Preimpresion, SL.

Respondek, Z. 2020. "Heat Transfer Through Insulating Glass Units Subjected to Climatic Loads." *Materials*, 13 (2): 286. Multidisciplinary Digital Publishing Institute. https://doi.org/10.3390/ma13020286.

Rodrigues, C., and F. Freire. 2017. "Building retrofit addressing occupancy: An integrated cost and environmental life-cycle analysis." *Energy and Buildings*, 140: 388–398. https://doi.org/10.1016/j.enbuild.2017.01.084.

Rogers, T.G., 2010. Considerations for the Condensation Resistance of Fenestration Assemblies. Proceedings of the Building Enclosure Science & Technology, 2.

Safavi, A., N. Maleki, and M. M. Doroodmand. 2010. "Single-walled carbon nanotubes as stationary phase in gas chromatographic separation and determination of argon, carbon dioxide and hydrogen." *Analytica Chimica Acta*, 675 (2): 207–212. https://doi.org/10.1016/j.aca.2010.07.019.

Samaitis, V., L. Mažeika, A. Jankauskas, R. Rekuvienė, V. Laurs, R. Bliūdžius, J. Kumžienė, and K. Banionis. 2022. "Hybrid ultrasonic technique for non-invasive evaluation of argon gas content in insulated glass units." *Energy and Buildings*, 266: 112123. https://doi.org/10.1016/j.enbuild.2022.112123.

Sasmal, S., S. Basu, C. V. V. Himakar, and T. Kundu. 2023. "Detection of interface flaws in Concrete-FRP composite structures using linear and nonlinear ultrasonics based techniques." *Ultrasonics*, 132: 107007. https://doi.org/10.1016/j.ultras.2023.107007.

Savić, J., D. Đurić-Mijović, and V. Bogdanović. 2013. "Architectural glass: Types, performance and legislation." *Facta universitatis - series: Architecture and Civil Engineering*, 11 (1): 35–45.

Selkowitz, S., R. Hart, and C. Curcija. 2018. "Breaking the 20 Year Logjam to Better Insulating Windows." https://doi.org/10.20357/B76K5K.

Souviron, J., G. van Moeseke, and A. Z. Khan. 2019. "Analysing the environmental impact of windows: A review." *Building and Environment*, 161: 106268. https://doi.org/10.1016/j.buildenv.2019.106268.

"Sparklike Handheld™." 2024. *Sparklike*. Accessed April 2, 2024. https://sparklike.com/en/product/sparklike-handheld/.

"Sparklike Laser Portable™ - Insulating Gas Measurement Device." 2024 *Sparklike*. Accessed April 19, 2024. https://sparklike.com/en/product/sparklike-laser-portable-2-1/.

"Sparklike Laser™ - Gas Testing | Inagas Ltd." 2024. Accessed July 16, 2024. https://www.inagas.com/gas-testing/sparklike-laser.php.

Summ, T., M. Ehrenwirth, C. Trinkl, W. Zörner, K. Pischow, R. Greenough, and M. Oyinlola. 2023. “Effect of argon concentration on thermal efficiency of gas-filled insulating glass flat-plate collectors.” *Applied Thermal Engineering*, 230: 120657. https://doi.org/10.1016/j.applthermaleng.2023.120657.

Tadeu, A. J. B., and D. M. R. Mateus. 2001. “Sound transmission through single, double and triple glazing. Experimental evaluation.” *Applied Acoustics*, 62 (3): 307–325. https://doi.org/10.1016/S0003-682X(00)00032-3.

Taskin, M., and Y. Kato. 2019. “Instant Gas Concentration Measurement Using Ultrasound From Exterior of a Pipe.” *IEEE Sensors Journal*, 19 (11): 4017–4024. https://doi.org/10.1109/JSEN.2019.2897736.

Van Den Bergh, S., R. Hart, B. P. Jelle, and A. Gustavsen. 2013. “Window spacers and edge seals in insulating glass units: A state-of-the-art review and future perspectives.” *Energy and Buildings*, 58: 263–280. https://doi.org/10.1016/j.enbuild.2012.10.006.

Watts, A., B. Shah, and R. Tenent. 2022. *Guidelines and Specifications for Enhanced Durability Evaluation of Insulating Glass and Vacuum Insulating Glass Units*. NREL/TP-5K00-83550, 1887442, MainId:84323.

Wolf, A. 2002. “Design and material selection factors that influence the service-life and utility value of dual-sealed insulating glass units.”

Wu, J., L. Wang, F. Du, G. Zhang, J. Niu, X. Rong, R. Song, H. Dong, J. Zhao, and Y. Li. 2023. “A two-DOF linear ultrasonic motor utilizing the actuating approach of longitudinal-traveling-wave/bending-standing-wave hybrid excitation.” *International Journal of Mechanical Sciences*, 248: 108223. https://doi.org/10.1016/j.ijmecsci.2023.108223.

Zhang, T. 2024. “Data Driven Framework for Structural Health Monitoring of Concrete using Elastic Wave Method.” thesis. University of Illinois at Chicago.

Zhu, X., L. J. Wang, X. L. Wang, Y. D. Zheng, and L. Luo. 2024. “Sound insulation performance and modal analysis of asymmetrical insulating laminated glass.” *Journal of Low Frequency Noise, Vibration and Active Control*, 43 (2): 846–862. SAGE Publications Ltd STM. https://doi.org/10.1177/14613484231214914.

Zier, M., P. Stenzel, L. Kotzur, and D. Stolten. 2021. “A review of decarbonization options for the glass industry.” *Energy Conversion and Management: X*, 10: 100083. https://doi.org/10.1016/j.ecmx.2021.100083.